Available online at www.sciencedirect.com
ScienceDirect
International Journal of Heat and Mass Transfer 51 (2008) 4743–4752
International Journal of HEAT and MASS TRANSFER
www.elsevier.com/locate/ijhmt

# Heat source identification and on-line temperature control by a Branch Eigenmodes Reduced Model

Etienne Videcoq [a,*], Olivier Quemener [a], Myriam Lazard [b], Alain Neveu [a]

[a] Laboratoire de Mécanique et d'Energétique d'Evry (LMEE) 40, rue du Pelvoux, 91 020 Evry Cedex, France
[b] Institut Supérieur d'Ingénierie de la Conception (InSIC) 27, rue d'Hellieule, 88 100 Saint-Dié-Des-Vosges, France

Received 20 September 2007; received in revised form 14 February 2008
Available online 21 April 2008

**Abstract**

This paper presents the advantages of a Branch Eigenmodes Reduced Model used in a control process of a heating system.

The experimental setup is a 3D heat conductive system in which a heat source is set. First, the reduced model is used to solve the non-linear Inverse Heat Conduction Problem: identification of the heat source strength variations from time-varying temperatures. Then, the reduced model is used to control hot points in the system. The objective of the method is to allow sequential temperature control by decreasing the computation time necessary for the simulation.


*Keywords:* 3D non-linear heat conduction; Inverse problem; Experiment; Function specification; Real time

## 1. Introduction

Among the several kinds of Inverse Heat Conduction Problems (IHCP) [1–4], this paper deals with the identification of a time varying heat source strength in a sequential manner from the knowledge of non-intrusive temperature measurements. To be used efficiently in industrial applications, the IHCP methods have to take into account complex and multi-dimensional geometries, to consider non-linear governing equations and to give a real-time estimation of the unknowns.

For multi-dimensional heat conduction problems, a detailed description of the studied system by classical modeling (finite elements,...) leads to a model of large dimension with a proportional requirement of computer time and memory. In order to lighten this drawback, boundary elements are very efficient [5]. As a matter of fact, this method does not require the complete mesh of the domain, but only the boundary mesh, which is particularly appropriate to the point heat source problem. Another solution consists in solving IHCP through a reduced model [6–8]. The method used in these cases to build the identified reduced model requires only decreasing temperature measurements. This experimental modeling, based on responses to step inputs, does not require a detailed model of the system, nor the knowledge of the thermal properties of the domain. Hence, this technique is particularly well adapted to the multi-dimensional IHCP. In [9,10], an inverse non-linear problem is solved either to determine the intrinsic diffusivity of semitransparent media or to estimate the temperature at the cutting tool's tip from two measured temperatures. Another kind of reduced model is implemented: the quadrupole formulation in the Laplace domain. The Levenberg–Marquardt algorithm is used to solve the inverse problem of parameters or functions estimation without any regularization procedure.

In non-linear cases, the inverse algorithms are iterative and require repeated computations of governing equations before getting a solution. Hence, it is necessary to adopt efficient techniques to overcome the large amount of

* Corresponding author. Tel.: +33 1 69 47 79 37; fax: +33 1 69 47 79 47.
*E-mail address:* E.Videcoq@iut.univ-evry.fr (E. Videcoq).

0017-9310/$ - see front matter © 2008 Elsevier Ltd. All rights reserved.
doi:10.1016/j.ijheatmasstransfer.2008.02.029

**Nomenclature**

| | |
|---|---|
| $\boldsymbol{B}\,(N,p)$ | command matrix |
| $c$ | volumetric heat capacity, J m$^{-3}$ K$^{-1}$ |
| $\boldsymbol{C}\,(N,N)$ | heat capacitance matrix |
| $h$ | convective exchange coefficient, W m$^{-2}$ K$^{-1}$ |
| $\boldsymbol{I}$ | identity matrix |
| $k$ | thermal conductivity, W m$^{-1}$ K$^{-1}$ |
| $\boldsymbol{K}\,(N,N)$ | heat conductance matrix |
| $n$ | order of RM |
| $N$ | order of DM |
| $nf$ | number of future times for specification function |
| $nt$ | number of time steps for simulation |
| $p$ | dimension of input vector |
| $q$ | dimension of output vector |
| $Q$ | heat source strength, W m$^{-3}$ |
| $R$ | electric resistance, Ω |
| $\boldsymbol{S}\,(q,N)$ | selection matrix |
| $t$ | time, s |
| $T$, $\dot{T}(N)$ | temperature vector, its derivative with respect to time, K, K s$^{-1}$ |
| $\underset{\sim}{U}\,(p)$ | input vector |
| $\underset{\sim}{\tilde{\boldsymbol{V}}}\,(N,n)$ | matrix of amalgam eigenmodes |
| vol | volume of the domain, m$^3$ |
| $\underset{\sim}{\tilde{X}}, \underset{\sim}{\dot{\tilde{X}}}(n)$ | RM state vector, its derivative with respect to time |
| $Y\,(q)$ | DM output vector |

*Abbreviations*

| | |
|---|---|
| BERM | Branch Eigenmodes Reduction Method |
| DHCP | Direct Heat Conduction Problem |
| DM | Detailed Model |
| IHCP | Inverse Heat Conduction Problem |
| RM | Reduced Model |

*Greek symbols*

| | |
|---|---|
| $\Gamma$ | system boundary |
| $\Delta t$ | time step, s |
| $\varepsilon$ | emissivity of the radiative surface |
| $\varepsilon_U$ | mean relative error for $U$ |
| $\varepsilon_{\text{vol}}$ | mean volume error, K |
| $\zeta$ | Steklov coefficient, J m$^{-2}$ K$^{-1}$ |
| $\lambda$ | eigenvalue |
| $\sigma$ | Stefan–Boltzmann constant, W m$^{-2}$ K$^{-4}$ |
| $\tau$ | time constant, s |
| $\Phi\,(N)$ | vector of thermal excitations |
| $\Omega$ | system domain |

*Subscripts*

| | |
|---|---|
| eq | equivalent |
| ext | exterior |
| vol | volume |

*Superscripts*

| | |
|---|---|
| $\underset{\sim}{\tilde{Y}}(q)$ | RM output vector |
| $\hat{}$ | estimated value |
| $^{\mathrm{T}}$ | transposition sign |
| $^{-1}$ | inverse of a matrix |

computation time and memory required to solve IHCP. A parameter estimation approach is presented in [11]. The aim of this study is to identify the location and the strength of multiple line heat sources placed in a homogeneous domain in a steady case. Due to the fact that the location of the line heat sources is unknown, the problem is non-linear. The boundary element method is used to build a direct model of the measurements. The parameter estimation approach allows to compute the confidence interval of the estimated locations and strengths. In [12], a sequential identification of a time-varying heat source strength is proposed for an inverse radiation problem employing an extended Kalman filter. The difficulty associated with the numerical solution of the covariance equation in the Kalman filter is overcome by converting the three-dimensional radiative transfer equation and heat conduction equation to a reduced order model by means of the Karhunen–Loève Galerkin procedure. In [13], the determination of heat sources and heat transfer coefficient for two-dimensional heat flow is carried out by a powerful method combining the conjugate gradient algorithm with the finite element technique. The results show that this technique is well adapted to perform inverse heat flow analysis for arbitrarily shaped bodies and non-linear problems with temperature dependent properties.

In the real time identification field of research, many studies have been carried out over the past few years. To obtain a solution of IHCP in real time, many difficulties occur. A first problem is that the sensors can be located far from the sources. Hence, due to the lagging and damping effects of the diffusion process, the thermal signal reaches the sensors with a delay. This problem, inherent to the geometry of the studied system, can be solved using future temperatures as a regularization procedure [14,15], but the identification of the unknowns in real time is not available, due to the physical delay. In configurations where the sensors are located near the sources, the addition of future temperatures is not physically necessary but the main difficulty lies in providing a stable solution with very short computation time. In [16], numerical transformation schemes between the time and Laplace domains to handle data that are not defined analytically are proposed for on-line estimation of the time-variant heat input to machine tool structures. An accelerated inverse numerical

Laplace transformation is developed to improve the numerical efficiency of the solver.

A non-linear model predictive control is proposed in [17]. The temperature control in long ducts is performed using a neural network model that avoids the spatial discretization and decreases significantly the computation time necessary for the solution of the optimization problem in real time.

The originality of our work lies in the fact that the non-linear three-dimensional IHCP is solved by a branch reduced model which requires a very low computation time and therefore allows to compute the whole temperature field at each time step.

The article is structured as follows: Section 2 describes the three-dimensional experimental device and its modeling. In Section 3, the principles of the Branch Eigenmodes Model Reduction and its application to the studied system are developed. The IHCP solution is then proposed in Section 4. Finally, Section 5 focuses on the sequential supervision of the temperature field in the domain.

## 2. Experimental device and modeling

### 2.1. Description of the 3D system

The proposed experimental device is used as a tool to validate the IHCP algorithms on a concrete application that contains many features of an industrial IHCP: 3D geometry, heat radiation, non-intrusive temperature measurements and transient case. The heterogeneous studied system is a parallelepiped block ($0.164\,\text{m} \times 0.098\,\text{m} \times 0.098\,\text{m}$) composed of steel ($k = 52\,\text{W m}^{-1}\,\text{K}^{-1}$, $c = 3.846 \times 10^6\,\text{J m}^{-3}\,\text{K}^{-1}$). The block is drilled in its length by two circular ducts (0.016 m in diameter) as shown in Fig. 1. The external surfaces of the block are insulated with ceramic sheets (0.024 m thick), except the two largest vertical faces, painted in black in order to increase the radiation heat transfer. A cylindrical heat source ($k = 20\,\text{W m}^{-1}\,\text{K}^{-1}$, $c = 4.235 \times 10^6\,\text{J m}^{-3}\,\text{K}^{-1}$, 20 mm in diameter and 60 mm long) is placed in the block as shown in Fig. 1.

The temperature measurements are given by an infrared camera positioned 1 m away from the surface $\Gamma_1$. The FLIR ThermoVision® A40 infrared camera features an uncooled microbolometer detector that delivers images with a resolution of 0.08 °C at 30 °C. Each thermal image is built from $320 \times 240$ individual picture elements that are sampled up to 60 times per second by the camera's on-board electronics and software, with a relative accuracy estimated to ±2%.

Fig. 2 presents a general view of the apparatus. The heat source is driven by a power modulator. Each channel of this power modulator can be adjusted from 1% to 100% of the maximum power of the thermal heating. The dissipated power in the source depends on the supply voltage and the mean resistance of the element ($R = 88\,\Omega$). The temperature dependence of the resistance is neglected for the power domain considered. The power modulator is controlled from a PC, as well as the power modulation timing. The source strength is then computed from the voltage and the heating element resistance $R$.

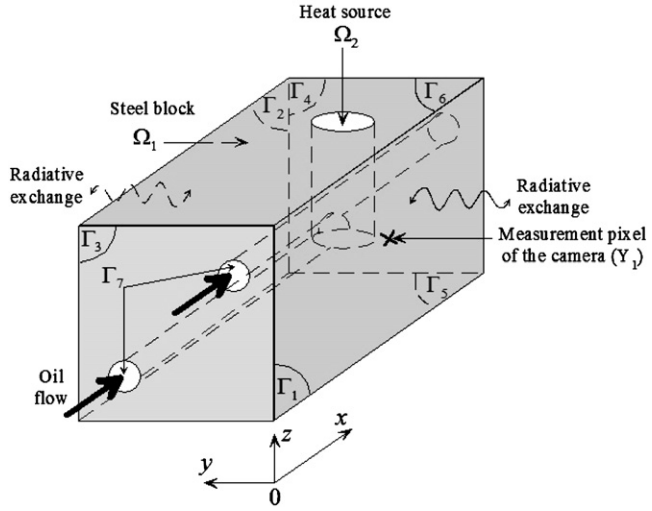


Fig. 1. The 3D diffusive system.

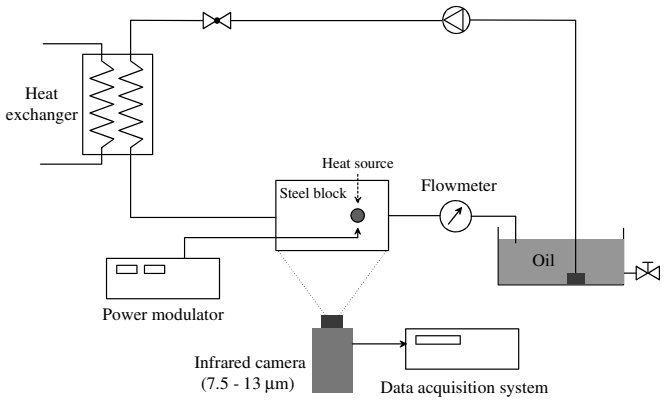


Fig. 2. Schematic representation of the experiment.

The heat extraction is realized with a high-rate oil flow in a closed circuit with a heat exchanger in such a way that the oil input temperature in the block is constant. In the ducts, the heat transfer coefficient between the solid and the oil is supposed to be constant because the flow rate is laminar and steady. The input and output oil temperatures are given by T-type thermocouples connected to the data acquisition system.

### 2.2. Modeling of the system

For the studied domains, the transient energy equations are

$$\forall M \in \Omega_1 \quad c_1 \frac{\partial T}{\partial t} = \nabla \cdot (k_1 \nabla T) \tag{1}$$

$$\forall M \in \Omega_2 \quad c_2 \frac{\partial T}{\partial t} = \nabla \cdot (k_2 \nabla T) + Q(t) \tag{2}$$

where $T(x,y,z,t)$ is the temperature and $Q$ represents the time dependent heat source strength.

Associated boundary conditions on the large faces are written:

$$\forall M \in \Gamma_i \quad (i = 1,2) \quad \boldsymbol{n} \cdot (k_1 \nabla T) = h_{\text{ext}}(T_{\text{ext}} - T) + \varepsilon\sigma(T_{\text{ext}}^4 - T^4) \tag{3}$$

where $T_{\text{ext}}$ is the ambient temperature, $h_{\text{ext}} = 8\ \text{W m}^{-2}\ \text{K}^{-1}$ is a convective exchange coefficient, $\varepsilon = 0.95$ is the emissivity of the black painted surfaces $\Gamma_1$ and $\Gamma_2$ and $\sigma$ is the Stefan–Boltzmann constant, $\boldsymbol{n}$ being the normal unit vector. The non-linear behavior of the system is due to the radiative exchange boundary condition.

On the partially insulated faces, boundary conditions satisfy the following equation:

$$\forall M \in \Gamma_i \quad (i = 3,4,5,6) \quad \boldsymbol{n} \cdot (k_1 \nabla T) = h_{\text{eq}}(T_{\text{ext}} - T) \tag{4}$$

$h_{\text{eq}} = 2.5\ \text{W m}^{-2}\ \text{K}^{-1}$ being the convective exchange coefficient between the partially insulated faces of the block and the ambient environment.

Concerning the oil ducts, the boundary conditions are written:

$$\forall M \in \Gamma_7 \quad \boldsymbol{n} \cdot (k_1 \nabla T) = h_{\text{oil}}(T_{\text{oil}} - T) \tag{5}$$

in which $h_{\text{oil}} = 40\ \text{W m}^{-2}\ \text{K}^{-1}$ is the convective exchange coefficient for the established laminar oil flow in the two ducts relative to the oil mean temperature $T_{\text{oil}}$.

The initial condition is given by $T(t=0) = 301$ K.

After spatial discretization using the finite element method with linear shape functions, Eqs. (1) and (2) and the associated boundary conditions can be written under matrix form:

$$\begin{cases} \boldsymbol{C}\dot{T}(t) = \boldsymbol{K}(T)T(t) + \Phi(t) + \boldsymbol{B}U(t) \\ Y(t) = \boldsymbol{S}T(t) \end{cases} \tag{6}$$

where $\boldsymbol{C}$ and $\boldsymbol{K}$ (dim. $N,N$) are respectively the heat capacitance and heat conductance matrices, $\Phi$ (dim. $N$) the vector of thermal excitations, $\boldsymbol{B}$ (dim. $N,p$) the command matrix relative to the input vector $U(t), T(t)$ (dim. $N$) the vector containing temperatures of all discretization nodes and $\dot{T}(t)$ the derivative of vector $T$ with respect to time. The matrix $\boldsymbol{S}$ (dim. $q,N$) is the observation matrix which allows us to select a part of the whole temperature field. The selection is contained in output vector $Y(t)$ (dim. $q$). Note that, in our case, $p = q = 1$, the input included in vector $U$ is the heat source strength $Q$ and only one temperature measurement point is used.

Concerning the time discretization, an implicit first-order scheme with adaptative time steps is implemented. The conjugate gradient method is used to solve the high dimensional non-linear system (temperature dependence of matrix $\boldsymbol{K}$). The initial time step is equal to 0.1 s and the time step for the storage of the temperatures is equal to $\Delta t = 10$ s.

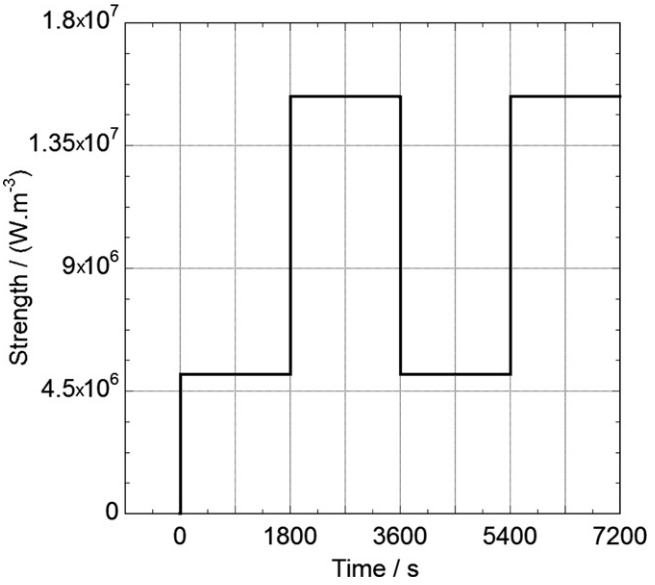


Fig. 3. Strength variation $Q(t)$ of the heat source.

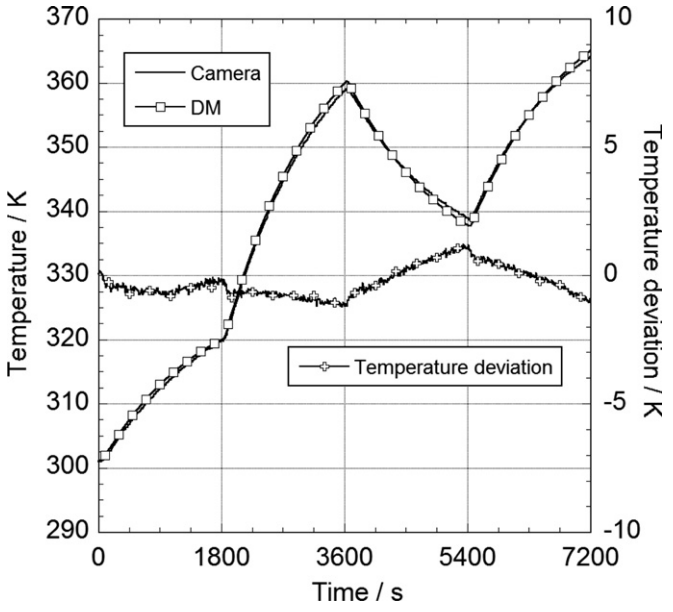


Fig. 4. Comparison of DM and camera temperature evolutions, $\Delta t = 10$ s.

Due to the 3D geometry and to the oil ducts and heat source cylindrical surfaces, a precise space discretization of the diffusive block is needed. After a mesh sensitivity study, the optimal mesh is found to be $N = 23{,}139$ nodes and 117,710 tetrahedra. The node corresponding to the point $Y_1$ of the middle of the radiative surface $\Gamma_1$ where the camera measures the temperature is the mesh node number 18,017. For the experiment and DM, the strength variation $Q(t)$ of the heat source is depicted in Fig. 3. In order to show the good agreement between DM and the experiment, the evolutions of the temperature of the point $Y_1$ are compared in Fig. 4. The temperature deviation does not exceed 1.2 K.

Due to the size of the matrices (dim. $N,N$), DM is very difficult to use to solve the inverse problem. The objective of the next part is to build a reduced model, computationally efficient.

## 3. Reduced model

### 3.1. Branch Eigenmodes Model Reduction

The technique used in this article in order to solve IHCP is the Branch Eigenmodes Reduction Method (BERM) [18–20].

The branch eigenmodes problem applied to a thermal system is defined by the following equations, where $c$ and $k$ are constant thermophysical properties

$$\forall M \in \Omega \quad \nabla \cdot (k \nabla V_i(M)) = \lambda_i c V_i(M) \tag{7}$$

$$\forall M \in \Gamma \quad -k \nabla V_i(M) \cdot \boldsymbol{n} = \lambda_i \zeta V_i(M) \tag{8}$$

Compared to the classical eigenmodes problem, the eigenvalue $\lambda_i$ ($= -1/\tau_i$, where $\tau_i$ is the time constant associated to the eigenmode $V_i$) appears in the boundary condition. Eq. (8) is called the Steklov boundary condition. In order to maintain the whole richness of the problem, an appropriate choice of the Steklov coefficient $\zeta$ is given by

$$\int_\Gamma \zeta \mathrm{d}M = \int_\Omega c \mathrm{d}M \tag{9}$$

In our case, Eq. (9) leads to a Steklov coefficient equal to 180,000 J m$^{-2}$ K$^{-1}$.

The computation of the eigenmodes using the Arnoldi technique [21] is then performed. Here, $N_\mathrm{E} = 4000$ eigenmodes are computed. Each eigenmode $V_i(M)$ is a spatial field. As it is not handy to represent them in a 3D view, they are not shown in this paper. Concerning the eigenvalues, the first eigenmode is associated to an infinite time constant, and the time constant of the 4000th eigenmode is equal to 1.3 s.

Hence, knowing the eigenmodes $V_i(M)$, the temperature field can be written as follows:

$$T(M,t) = \sum_{i=1}^{N_\mathrm{E}} X_i(t) V_i(M) \tag{10}$$

where $N_\mathrm{E}$ ($\leqslant N$) is the number of calculated eigenmodes and $X_i(t)$ the state vector related to the eigenmode $V_i(M)$.

The objective of BERM is to compute the temperature field, with the same equation as Eq. (10), but with less eigenmodes, in order to decrease the computation time:

$$\widetilde{T}(M,t) = \sum_{i=1}^{n} \widetilde{X}_i(t) \widetilde{V}_i(M) \cong \sum_{i=1}^{N_E} X_i(t) V_i(M) \tag{11}$$

with $n \ll N_\mathrm{E}$ and $\widetilde{V}_i$ being the $i$th amalgam eigenmode of the reduced model, computed with the simplified amalgam method [20]. The objective is to bring together the eigenmodes into $n$ subspaces ($n \ll N$), where $n$ is the order of RM. First, the $n$ major eigenmodes are chosen. Then, the distribution of the minor eigenmodes into the $n$ subspaces is performed, according to a measure of the reduction error [19].

Finally, the $n$ amalgam eigenmodes are brought together into matrix $\widetilde{\boldsymbol{V}}$ (dim. $N,n$) and RM can be expressed under matrix form:

$$\begin{cases} \widetilde{\boldsymbol{V}}^\mathrm{T} \boldsymbol{C} \widetilde{\boldsymbol{V}} \dot{\widetilde{X}}(t) = \widetilde{\boldsymbol{V}}^\mathrm{T} \boldsymbol{K}(\widetilde{T}) \widetilde{\boldsymbol{V}} \widetilde{X}(t) + \widetilde{\boldsymbol{V}}^\mathrm{T} \boldsymbol{\Phi}(t) + \widetilde{\boldsymbol{V}}^\mathrm{T} \boldsymbol{B} U(t) \\ \widetilde{Y}(t) = \boldsymbol{S} \widetilde{\boldsymbol{V}} \widetilde{X}(t) \end{cases} \tag{12}$$

with $\widetilde{T} = \widetilde{\boldsymbol{V}} \widetilde{X}$. These equations can be written under a more convenient form:

$$\begin{cases} \boldsymbol{L} \dot{\widetilde{X}}(t) = \boldsymbol{M}(\widetilde{T}) \widetilde{X}(t) + \widetilde{\boldsymbol{V}}^\mathrm{T} \boldsymbol{\Phi}(t) + \boldsymbol{G} U(t) & \text{(a)} \\ \widetilde{Y}(t) = \boldsymbol{H} \widetilde{X}(t) & \text{(b)} \end{cases} \tag{13}$$

where

$$\begin{cases} \boldsymbol{L} = \widetilde{\boldsymbol{V}}^\mathrm{T} \boldsymbol{C} \widetilde{\boldsymbol{V}} \\ \boldsymbol{M}(\widetilde{T}) = \widetilde{\boldsymbol{V}}^\mathrm{T} \boldsymbol{K}(\widetilde{T}) \widetilde{\boldsymbol{V}} \\ \boldsymbol{G} = \widetilde{\boldsymbol{V}}^\mathrm{T} \boldsymbol{B} \\ \boldsymbol{H} = \boldsymbol{S} \widetilde{\boldsymbol{V}} \end{cases} \tag{14}$$

Eq. (13a) is a system of reduced order $n$. Matrices $\boldsymbol{L}$ and $\boldsymbol{M}$ have low dimensions $(n,n)$. As for DM, an implicit first-order scheme with adaptative time steps is implemented. The LDLT factorization method, well adapted to the reduced-order matrices, is used to solve the system.

### 3.2. Results and discussion

Different reduced models are tested ($n = 5, 10, 20, 40, 60, 80$ and 100). The heat strength $Q(t)$ is represented in Fig. 3. The direct simulations are carried out using a storage time step equal to 10 s ($nt = 721$). Table 1 summarizes the smallest time constant $\tau_\mathrm{min}$ of each reduced model and the CPU time necessary for the complete direct simulation. Note that the abbreviation RM5 refers to $n = 5$.

Concerning the smallest time constant of each RM, when $n$ increases, $\tau_\mathrm{min}$ decreases, allowing to reproduce fast dynamics.

Regarding the computation time, the simulations have been performed on the same computer. It clearly appears that RM computation times are very small (divided by a factor 13 to 694 (for RM5) compared to DM in the present study).

Note that the use of RM provides a large reduction ratio, what induces an important gain in computer memory.

In order to compare the DM and RM responses, a mean volume error is defined as follows:

$$\varepsilon_\mathrm{vol} = \frac{1}{nt \times \mathrm{vol}} \sum_{i=1}^{nt} \int_\Omega \mathrm{abs}\Big(T_i(M) - \widetilde{T}_i(M)\Big) \mathrm{d}v \tag{15}$$

where $T$ and $\widetilde{T}$ are respectively the DM and RM temperature fields, $nt$ the number of time steps and vol the volume of the domain.

Table 1
Smallest time constant and CPU time for each model

| Model | DM | RM5 | RM10 | RM20 | RM40 | RM60 | RM80 | RM100 |
|---|---|---|---|---|---|---|---|---|
| $\tau_{min}$ (s) | – | 62.5 | 25.5 | 9.0 | 6.2 | 3.1 | 3.1 | 3.1 |
| CPU time (s) | 3471 | 5 | 9 | 22 | 61 | 116 | 189 | 271 |

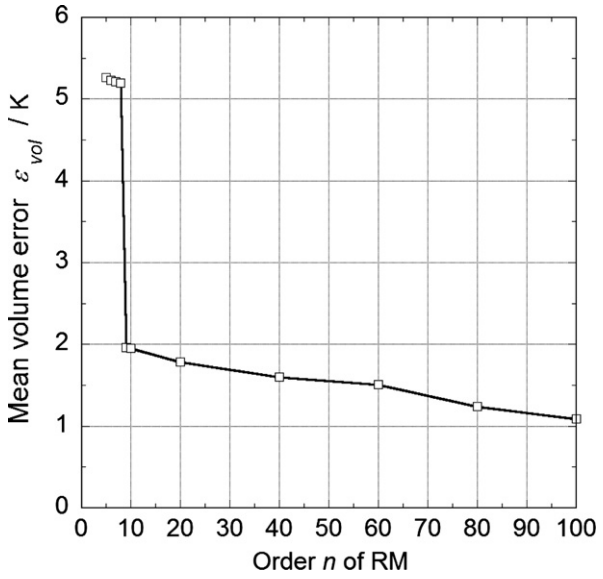


Fig. 5. Evolution of the mean volume error $\varepsilon_{vol}$ versus RM order $n$.

The evolution of $\varepsilon_{vol}$ is represented in Fig. 5 for different orders $n$ of RM. It can be underlined that the increase of $n$ leads to an important improvement of the accuracy of RM.

The comparison of the temperature evolutions between DM and RM5 and between DM and RM100 for the point $Y_1$ are shown respectively in Fig. 6a and b. As expected, RM100 gives the best results. The temperature deviation does not exceed 0.5 K, in this case.

## 4. Inverse problem

### 4.1. Inverse algorithm

RM is now used in order to solve IHCP. The procedure is sequential. Knowing the input vector $U(k)$ at the time step $k$, the aim is to identify the vector $U(k+1)$ from temperatures at the time step $(k+1)$.

Using an implicit time discretization, Eq. (13a) leads to

$$\widetilde{X}(k+1) = \left[\boldsymbol{I} - \Delta t \boldsymbol{L}^{-1}\boldsymbol{M}(\widetilde{T})\right]^{-1}\left[\widetilde{X}(k) + \Delta t \boldsymbol{L}^{-1}\widetilde{\boldsymbol{V}}^{\mathrm{T}}\Phi(k+1) + \Delta t \boldsymbol{L}^{-1}\boldsymbol{G}U(k+1)\right] \tag{16}$$

Hence, it ensues a relation between RM output vector and the input vector $U(k+1)$:

$$\widetilde{Y}(k+1) = \boldsymbol{H}\mathscr{G}U(k+1) + \boldsymbol{H}[\mathscr{M}\widetilde{X}(k) + \mathscr{L}\Phi(k+1)] \tag{17}$$

with the following matrices:

$$\begin{cases} \mathscr{M} = \left[\boldsymbol{I} - \Delta t \boldsymbol{L}^{-1}\boldsymbol{M}(\widetilde{T})\right]^{-1} \\ \mathscr{L} = \mathscr{M}\Delta t \boldsymbol{L}^{-1}\widetilde{\boldsymbol{V}}^{\mathrm{T}} \\ \mathscr{G} = \mathscr{M}\Delta t \boldsymbol{L}^{-1}\boldsymbol{G} \end{cases} \tag{18}$$

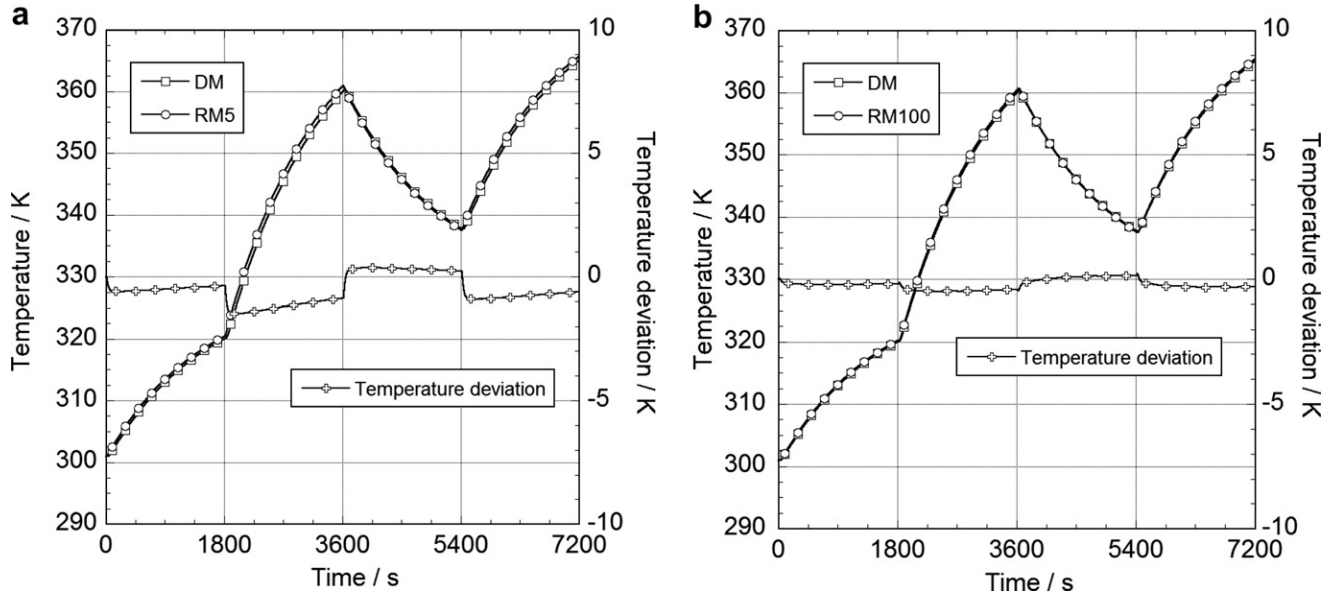


Fig. 6. Comparison of DM and RM temperature evolutions at the point $Y_1$. (a) Deviation between DM and RM5. (b) Deviation between DM and RM100.

In order to take into account the lagging and damping effects of the diffusion process, it is necessary to obtain information using future time steps [6,14]. A function specification is introduced. A temporary assumption is made on the additional unknowns: $U(k+1+1),\ldots,U(k+1+nf)$, where $nf$ is the number of future time steps. In this study, a constant value of $U$ is chosen:

$$U(k+1+i) = U(k+1) = \text{constant for } 1 \leqslant i \leqslant nf \quad (19)$$

The addition of future time steps leads to the resolution of a system of $(nf+1)\times q$ equations where $q$ is the number of measurements. In this study, $q=1$, because only one pixel of the camera view is used.

Hence, at each time step, the temperature measurements vector $\boldsymbol{Y}^*$ contains $(nf+1)$ rows, as follows:

$$\boldsymbol{Y}^* = \begin{bmatrix} Y^*(k+1) \\ Y^*(k+2) \\ \vdots \\ Y^*(k+nf+1) \end{bmatrix} \quad (20)$$

The system to solve is then overdetermined. The aim is to identify the pseudo-solution $\widehat{U}(k+1)$ of IHCP, such as $\boldsymbol{Y}^* - \widetilde{\boldsymbol{Y}} \cong 0$, where $\widetilde{\boldsymbol{Y}}$ is the temperature vector computed by RM. This condition can be written, according to Eq. (17):

$$\boldsymbol{Y}^* - (\boldsymbol{C}\widehat{U}(k+1) + \boldsymbol{D}) \cong 0 \quad (21)$$

with the following matrices:

$$\boldsymbol{C} = \begin{bmatrix} \boldsymbol{H}\mathscr{G} \\ \boldsymbol{H}[\mathscr{G} + \mathscr{M}\mathscr{G}] \\ \vdots \\ \boldsymbol{H}\left[\boldsymbol{I} + \sum_{j=1}^{nf} \mathscr{M}^j\right]\mathscr{G} \quad \forall\, nf \geqslant 1 \end{bmatrix} \quad (22)$$

$$\boldsymbol{D} = \begin{bmatrix} \boldsymbol{H}\left[\mathscr{M}\widetilde{X}(k) + \mathscr{L}\Phi(k+1)\right] \\ \boldsymbol{H}\left[\mathscr{M}^2\widetilde{X}(k) + \mathscr{M}\mathscr{L}\Phi(k+1) + \mathscr{L}\Phi(k+2)\right] \\ \vdots \\ \boldsymbol{H}\left\{\mathscr{M}^{nf+1}\widetilde{X}(k) + \left[\sum_{j=0}^{nf} \mathscr{M}^j\mathscr{L}\Phi(k+nf+1-j)\right]\right\} \end{bmatrix} \quad (23)$$

According to Eq. (21), the inversion procedure, using the least square method, leads to the sequential solution:

$$\widehat{U}(k+1) = (\boldsymbol{C}^{\mathrm{T}}\boldsymbol{C})^{-1}\boldsymbol{C}^{\mathrm{T}}(\boldsymbol{Y}^* - \boldsymbol{D}) \quad (24)$$

Using RM, the IHCP can be solved while it is impossible to do by DM due to the size of the matrices to invert. Note that the inverse of a squared matrix $(23139\times 23139)$ requires

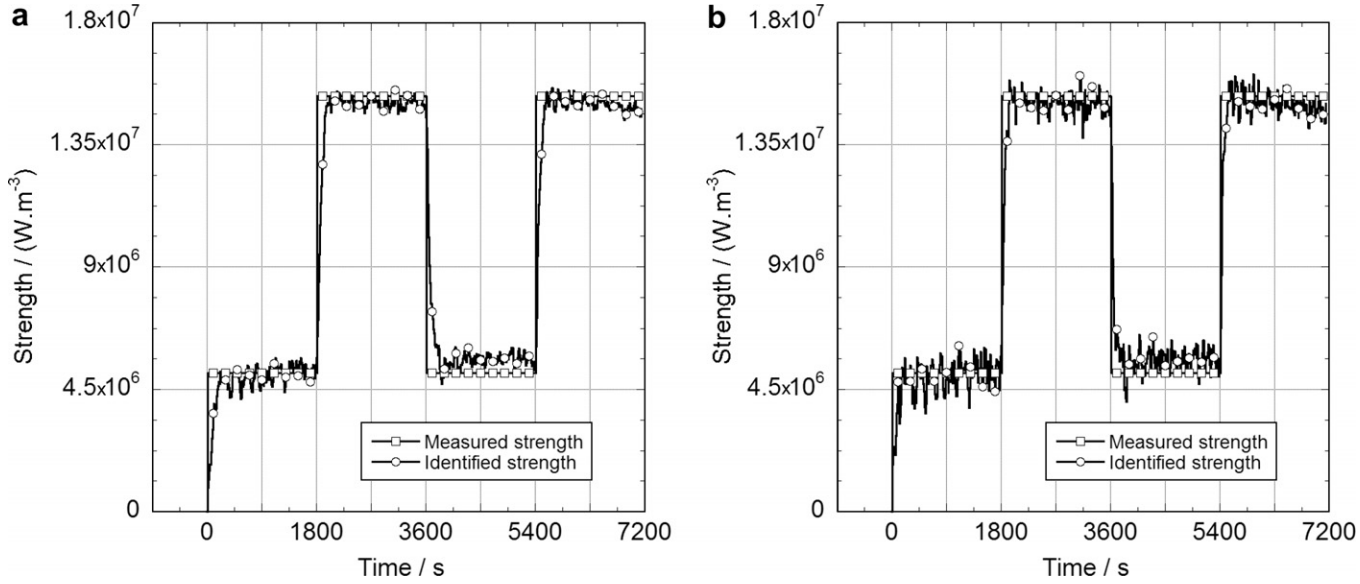


Fig. 7. Identification of $Q(t)$ with $nf=5$, $\Delta t = 10$ s. (a) Identification through RM5. (b) Identification through RM100.

Table 2
Comparison of inversion results for different RMs, with $nf=5$

| Model | RM5 | RM10 | RM20 | RM40 | RM60 | RM80 | RM100 |
|---|---|---|---|---|---|---|---|
| $\varepsilon_U$ (%) | 8.09 | 8.15 | 8.36 | 9.40 | 7.79 | 8.24 | 7.86 |
| CPU time per step (s) | 0.01 | 0.02 | 0.05 | 0.15 | 0.28 | 0.44 | 0.65 |

4.2 Gb of storage and personal computers have limited amount of random access memory (2 Gb in our case).

### 4.2. Results and discussion

The heat source is submitted to the strength variation represented in Fig. 3. The temperature is measured at point $Y_1$ using the infrared camera with $\Delta t = 10$ s. These noisy temperatures measured by the camera are used in the inverse procedure, without any filtering procedure. The objective is to be able to identify the value of $Q$ included in vector $U(k+1)$ at each time step $(k+1)$, i.e. during a maximum duration of 10 s. It should be noted that point $Y_1$ is located far from the heat source. Hence, during the first 60 s of the history, the temperature is always equal to the initial one: 301 K. Due to the lagging effect of the diffusion process, it is necessary to use future time steps. As the time step is equal to 10 s, the number of future temperatures is, at least, $nf = 5$.

Many inversion tests have been carried out using different reduced models. The inversion results, as well as the real strength are presented in Fig. 7a and b for $nf = 5$. The results are quite satisfactory except for some oscillations, probably due to the oscillations in the temperature measurements of the camera, as shown in Fig. 4. It clearly appears in Fig. 7a that RM5 reduces the oscillations in the identified values of $Q(t)$, what means that RM5 acts as a regularization procedure in IHCP.

Table 2 shows the computation time per time step and the mean relative error $\varepsilon_U$, defined as follows:

$$\varepsilon_U(\%) = \frac{1}{(nt - nf - 1)} \times \sum_{k=1}^{nt-nf-1} \left[ \mathrm{abs}\left( \frac{U_k - \widehat{U}_k}{U_k} \right) \times 100 \right] \quad (25)$$

in which $U$ is the measured strength and $\widehat{U}$ the identified one. Of course, in real applications, $\varepsilon_U$ can not be computed. This criterion is given here as supplementary information.

It can be underlined that the increase of RM order does not improve significantly the inversion results, contrary to the direct problem.

Moreover, due to the low dimension of RM, CPU time is very small, and the inversion of the matrix $[\boldsymbol{I} - \Delta t \boldsymbol{L}^{-1} \boldsymbol{M}(\widetilde{T})]$ of Eq. (18) is numerically practicable.

## 5. Sequential temperature control

The heat source strength being identified, the objective is to compute the whole temperature field $\widetilde{T}_{\widehat{U}}(t)$ with a computationally efficient procedure. Hence, RM is used a second time to solve DHCP at each time step in order to supervise the hot zones of the domain (hot points, dilation). The general procedure is represented in Fig. 8. At each time step $k$, the computer saves the temperatures $Y^*$ measured by the infrared camera. From the time $(nf+1) \times \Delta t$, the identification procedure begins. For example, for $nf = 2$, the temperatures $Y^*(\Delta t)$, $Y^*(2 \times \Delta t)$, $Y^*(3 \times \Delta t)$ are used to identify $\widehat{U}(\Delta t)$ by RM. Knowing $\widehat{U}(\Delta t)$, RM is then used in a direct procedure to compute $\widetilde{T}_{\widehat{U}}(\Delta t)$. The duration of this procedure (IHCP and DHCP) must not exceed the time step of the temperature acquisition because the procedure must run at each time step. The different reduced models are tested.

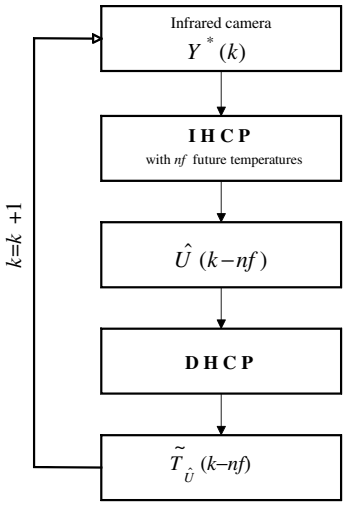


Fig. 8. The steps of the sequential procedure.

For illustration, the isothermal lines at the cross-section $x = 0.082$ m and for the time $t = 7000$ s are represented in Fig. 9. Fig. 9a shows the temperatures computed by RM5. The procedure (identification and rebuilding of the whole temperature field) needs 0.01 s per time step, as shown in Table 2. Fig. 9b depicts the temperatures computed by RM100. This reduced model requires more CPU time: 0.65 s per time step. Nevertheless, this duration is lower than the acquisition time step ($\Delta t = 10$ s). It is easy to remark that, even if RM5 and RM100 give approximately the same results for $\widehat{U}(t)$, the rebuilt temperature fields are different. Not enough spatial information is included in RM5 to rebuild an accurate temperature field. It yields a mean temperature for the cross-section.

In order to compare the results, Fig. 9c shows the temperature field computed by DM and the exact heat source strength. This figure confirms that the temperature levels given by RM100 are reasonably accurate. The hottest zone is located in the middle of the upper surface.

For comparison, Fig. 9d shows the temperature field computed with RM5 and the exact input $U(t)$. The mean volume error between DM and RM5 is equal to 5.26 K, as shown in Fig. 5. It can be underlined that the temperature levels are approximately the same than those represented in Fig. 9a. These figures confirm that, even if IHCP solutions can be obtained using a very low order RM, this RM is not sufficiently accurate to allow the sequential temperature control and the supervision of the hot points in the domain.

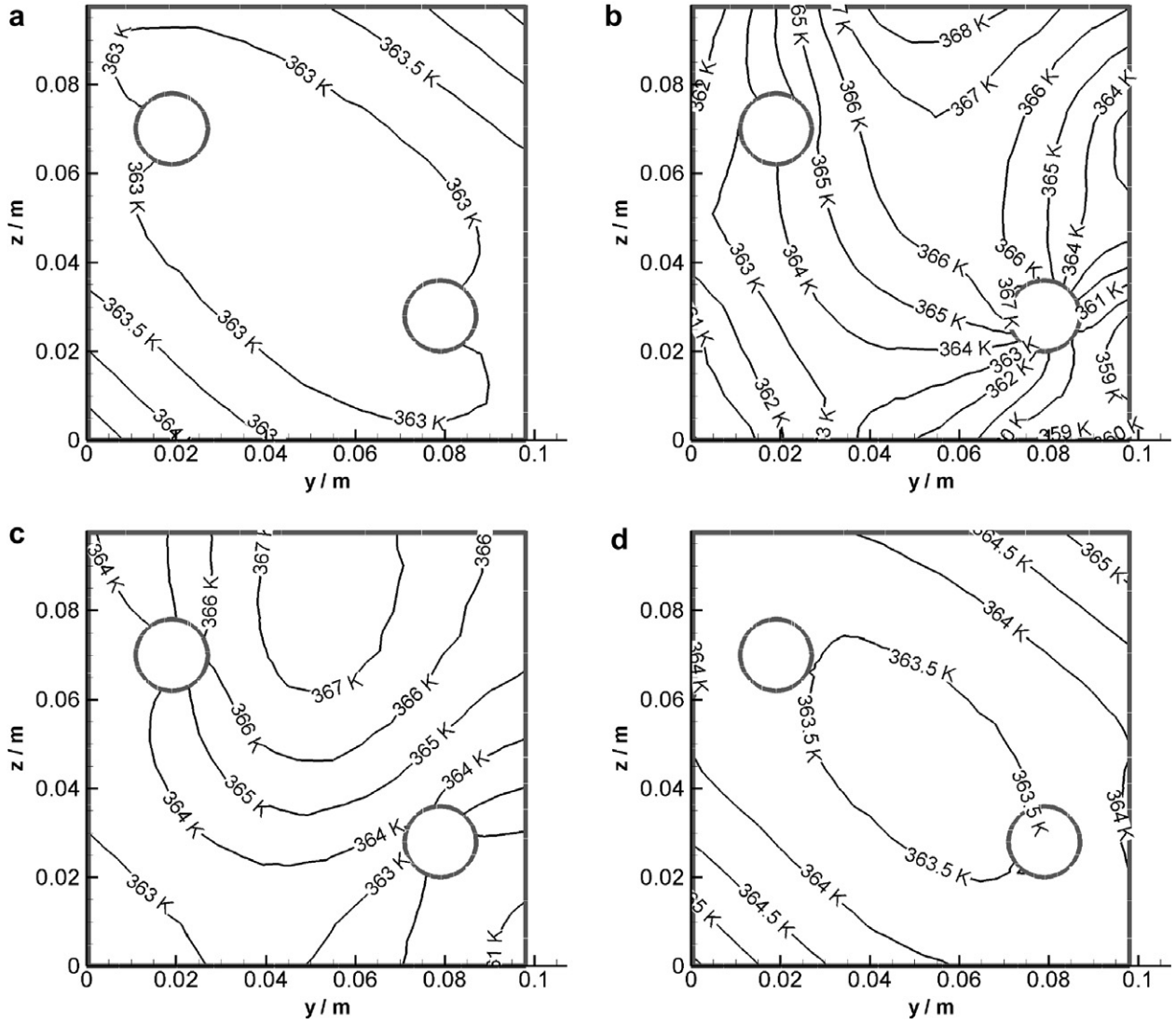


Fig. 9. Isothermal lines at the cross-section $x = 0.082$ m and $t = 7000$ s. (a) Temperature field computed with RM5 and $\widehat{U}(t)$ of Fig. 7a. (b) Temperature field computed with RM100 and $\widehat{U}(t)$ of Fig. 7b. (c) Temperature field computed with DM and the real input $U$(t). (d) Temperature field computed with RM5 and the real input $U$(t).

## 6. Conclusion

This study deals with the identification of a heat source strength from non-intrusive temperature measurements. The heat source is located in a steel block and the measurements are performed on a radiative surface of the block. Due to the high dimensional matrices, the detailed model of the system can not be used in order to solve IHCP. The use of a Branch reduced model for the solution of IHCP is then introduced. The method is sequential and includes the regularization with the function specification technique. The influence of the reduction order is analyzed for both DHCP and IHCP. The technique gives accurate results and is particularly robust in multi-dimensional IHCPs. Moreover, the method is computationally efficient (only 0.65 s at each time step for RM100). It becomes then possible to compute the complete temperature field, knowing the estimated input vector, at each time step, in order to supervise hot zones in the domain and to evaluate the non-linear matrices ($\boldsymbol{K}$ in our case).

Further developments of this approach focus on the coupling of two reduced models: the first one for the solid part and the second one for the fluid (for instance, the oil flow).

## References

[1] J.V. Beck, B. Blackwell, C.R. St. Clair, Inverse Heat Conduction: ill-posed Problems, Wiley, NY, 1985, pp. 108–160.
[2] J.V. Beck, B. Blackwell, A. Haji-Sheikh, Comparison of some inverse heat conduction methods using experimental data, Int. J. Heat Mass Tran. 39 (1996) 3649–3657.
[3] O.M. Alifanov, E.A. Artyukhin, S.V. Rumyantsev, Extreme Methods for Solving Ill Posed Problems with Applications to Inverse Heat Transfer, Begell House, NY, 1995, pp. 152–215.
[4] A.M. Osman, K.J. Dowding, J.V. Beck, Numerical solution of the general two-dimensional inverse heat conduction problem, ASME J Heat Tran. 119 (1997) 38–45.

[5] C. Le Niliot, The boundary-element method for the time-varying strength estimation of point heat sources: application to a two-dimensional diffusion system, Numer. Heat Tran., Part B 33 (1998) 301–321.
[6] E. Videcoq, D. Petit, A. Piteau, Experimental modeling and estimation of time varying thermal sources, Int. J. Therm. Sci. 42 (2003) 255–265.
[7] M. Girault, D. Petit, E. Videcoq, The use of model reduction and function decomposition for identifying boundary conditions of a linear thermal system, Inv. Prob. Eng. 11 (2003) 425–455.
[8] M. Girault, D. Petit, Identification methods in non-linear heat conduction, Part II: inverse problem using a reduced model, Int. J. Heat Mass Tran. 48 (2005) 119–133.
[9] M. Lazard, S. André, D. Maillet, D. Baillis, A. Degiovanni, Flash experiment on a semitransparent material: interest of a reduced model, Inv. Prob. Eng. 9 (2001) 413–429.
[10] M. Lazard, P. Corvisier, Modeling of a tool during turning. Analytical prediction of the temperature and of the heat flux at the tool's tip, Appl. Therm. Eng. 24 (2004) 839–849.
[11] C. Le Niliot, F. Lefèvre, A parameter estimation approach to solve the inverse problem of point heat sources identification, Int. J. Heat Mass Tran. 47 (2004) 827–841.
[12] H.M. Park, M.C. Sung, Sequential solution of a three-dimensional inverse radiation problem, Comput. Meth. Appl. Mech. Eng. 192 (2003) 3689–3704.
[13] R. Abou Khachfe, Y. Jarny, Determination of heat sources and heat transfer coefficient for two-dimensional heat flow – numerical and experimental study, Int. J. Heat Mass Tran. 44 (2001) 1309–1322.
[14] G. Blanc, M. Raynaud, T.H. Chau, A guide for the use of the function specification method for 2D Inverse Heat Conductions Problems, Int. J. Therm. Sci. 37 (1998) 17–30.
[15] S.M. Lin, C.K. Chen, Y.T. Yang, A modified sequential approach for solving Inverse Heat Conduction Problems, Int. J. Heat Mass Tran. 47 (2004) 2669–2680.
[16] M.H. Attia, S. Fraser, M.O.M. Osman, On-line estimation of time-variant thermal load applied to machine tool structures using a s-domain inverse solution, Int. J. Mach. Tool Manuf. 39 (1999) 985–1000.
[17] E. Aggelogiannaki, H. Sarimveis, D. Koubogiannis, Model predictive temperature control in long ducts by means of a neural network approximation tool, Appl. Therm. Eng. 27 (2007) 2363–2369.
[18] A. Neveu, K. El Khoury, B. Flament, Simulation de la décomposition non linéaire en régime variable: décomposition sur les modes de branche, Int. J. Therm. Sci. 38 (1999) 289–304.
[19] E. Videcoq, M. Girault, A. Neveu, O. Quemener, D. Petit, Comparison of two non-linear model reduction techniques: the modal identification method and the Branch Eigenmodes Reduction Method, Num. Heat Tran., Part B 9 (2006) 537–558.
[20] O. Quemener, A. Neveu, E. Videcoq, A specific reduction method for the branch modal formulation: application to a highly non-linear configuration, Int. J. Therm. Sci. 46 (2007) 890–907.
[21] W.E. Arnoldi, The principle of minimized iterations in the solution of the matrix eigenvalues problem, Quarterly Appl. Math. 9 (1951) 17–29.